DOI: 10.1002/chem.200702053

Clusterization, Electrophoretic Deposition, and Photoelectrochemical Properties of Fullerene-Functionalized Carbon Nanotube Composites

Tomokazu Umeyama,[a] Noriyasu Tezuka,[a] Mitsuru Fujita,[a] Shinya Hayashi,[a] Naoki Kadota,[a] Yoshihiro Matano,[a] and Hiroshi Imahori*[a, b, c]

Abstract: We have successfully developed a new methodology for the self-organization of C_{60} molecules on the sidewall of carbon nanotubes for use in photoelectrochemical devices. Novel nanocarbon composites of fullerene (e.g., C_{60}) and highly soluble, chemically functionalized single-walled carbon nanotubes (f-SWNT) have been prepared by the rapid injection of a poor solvent (e.g., acetonitrile) into a mixed solution of C_{60} and f-SWNT in *o*-dichlorobenzene. Measurements by using scanning electron microscopy of cast samples revealed that the composites are categorized into three groups; i) f-SWNT bundles covered with layers of C_{60} molecules, ii) round, large C_{60} clusters (sizes of 500–1000 nm) containing f-SWNT, and iii) typical, round C_{60} clusters (sizes of 150–250 nm). The electrophoretic deposition of the composites onto a nanostructured SnO_2 electrode yielded the hierarchical film with a gradient composition depending on the difference in the mobilities of C_{60} and f-SWNT during the electrophoretic process. The composite film exhibited an incident photon-to-photocurrent efficiency as high as 18% at $\lambda =$ 400 nm under an applied potential of 0.05 V vs. SCE. The photocurrent generation efficiency is the highest value among carbon nanotube-based photoelectrochemical devices in which carbon nanotubes are deposited electrophoretically, electrostatically or covalently onto semiconducting electrodes. The highly aligned structure of C_{60} molecules on f-SWNT can rationalize the efficient photocurrent generation. The results obtained here will provide valuable information on the design of carbon nanotube-based molecular devices.

Keywords: chemical functionalization · electrophoretic deposition · fullerenes · nanotubes · photoelectro chemistry

Introduction

Single-walled carbon nanotubes (SWNT) have been regarded as potential materials for highly efficient transportation of charges in optoelectronic and photovoltaic devices, owing to their one-dimensional structure and unique electronic and photophysical properties. However, the poor solubility of SWNT in aqueous or organic solvents, owing to their extremely strong π–π interactions has resulted in a marked impediment to their applications. Covalent chemical functionalization is one of the promising approaches to impart sufficient solubility to SWNT.[1–7] Extensive sidewall functionalization is known to disrupt the conjugated π-systems of SWNT.[1,3–7] On the other hand, shortened SWNT by acid treatment largely preserves the characteristic electronic structure, since the chemical functionalization (e.g., by a carboxylic group) localizes at terminals and defect sites of the nanotube structure and in turn most of the sidewall remains intact.[2] Noncovalent functionalization using hydrophobic interactions[8–10] in aqueous solvents and π–π interactions in aqueous or organic solvents[11–13] is an alternative approach because it can provide a general method of dissolving SWNT without altering the electronic structure. Various π electron-donating compounds including pyrenes,[11] porphyrins,[12] and π-conjugated polymers[13] have been employed to

[a] Dr. T. Umeyama, N. Tezuka, M. Fujita, S. Hayashi, N. Kadota, Prof. Y. Matano, Prof. H. Imahori
Department of Molecular Engineering
Graduate School of Engineering, Kyoto University
Nishikyo-ku, Kyoto 615–8510 (Japan)
Fax.: (+81) 75-383-2571
E-mail: imahori@scl.kyoto-u.ac.jp

[b] Prof. H. Imahori
Institute for Integrated Cell-Material Sciences (iCeMS)
Kyoto University
Nishikyo-ku, Kyoto 615–8510 (Japan)

[c] Prof. H. Imahori
Fukui Institute for Fundamental Chemistry
Kyoto University, 34–4, Takano-Nishihiraki-cho
Sakyo-ku, Kyoto 606–8103, Japan

Supporting information for this article is available on the WWW under http://www.chemistry.org or from the author.

interact with SWNT, leading to formation of supramolecular complexes in aqueous or organic media under ultrasonication. Thus, the complexation of π electron-rich compounds with SWNT imparts moderate solubility to SWNT. Nevertheless, integration of such complexes into photoelectrochemical and photovoltaic devices has not given satisfactory results, owing to the insufficient debundling of SWNT by the π electron-rich compounds.[14]

Three-dimensional structural fullerenes are carbon allotropes that exhibit peculiar electron transfer (ET) properties. There has been intensive research on photovoltaic systems utilizing fullerenes and their derivatives as acceptors,[15,16] because the small reorganization energies of fullerenes in ET lead to remarkable acceleration of photoinduced charge separation (CS) and of charge shift as well as deceleration of charge recombination (CR).[17] With these in mind, the arrangement of fullerene molecules along SWNT is an attractive strategy to attain efficient transportation of charges in photoelectrochemical and photovoltaic devices. Examples of such arrangements, however, are almost limited to fullerene-encapsulated SWNT (bucky-peapods),[18,19] which are insoluble in organic solvents, making it difficult to apply them to molecular devices. No fullerene-SWNT composites utilizing the π–π interactions between fullerenes and the external sidewall of SWNT have been isolated and investigated, owing to the poor solubility of the composites in organic solvents. Although there are several examples of ternary composites comprising of C_{60}, SWNT, and other π-conjugated compounds,[20] the interaction between C_{60} and SWNT has attracted less attention in the complicated ternary systems.

Recently, Mitra et al. reported the formation of a C_{60}-SWNT supramolecular complex in toluene/H_2O or toluene/EtOH (v/v = 1/25) by using microwave irradiation.[21] They spin-coated the composite solution with poly(3-hexylthiophene) (P3HT) to an indium-tin-oxide (ITO) electrode to fabricate bulk heterojunction solar cells. The power conversion efficiency (0.57%) was found to be improved compared to the reference cell, which comprised of P3HT and C_{60} without SWNT under their experimental conditions, but is much smaller than the typical value (3–5%) of P3HT-C_{60} bulk heterojunction solar cells.[22] Thus, the relationship between the structure and photovoltaic properties of C_{60}-SWNT composites remains elusive.

Here we report on a novel strategy for the arrangement of C_{60} molecules on the external surface of a SWNT. First, acid treatment cuts the pristine SWNT (p-SWNT) to yield shortened SWNT (s-SWNT) with carboxylic groups at the open ends and defect sites (Scheme 1, step 1).[2] The s-SWNT are then functionalized with a sterically hindered amine (i.e., swallow-tailed secondary amine) to yield functionalized SWNT (f-SWNT), soluble in organic solvents (step 2). Finally, a poor solvent (i.e., acetonitrile) is rapidly injected into a mixture of C_{60} and f-SWNT in a good solvent (such as *o*-dichlorobenzene, ODCB), resulting in the formation of composite clusters of C_{60} and f-SWNT ($(C_{60}+$ f-SWNT$)_m$).[23] We expected that lyophobic interactions between C_{60}-f-SWNT and the mixed solvent as well as the π–π interaction between C_{60} molecules and between C_{60} and f-SWNT would lead to the desirable arrangement of C_{60} molecules on the external surface of the SWNT in the mixed solvent (step 3). We also describe photoelectrochemical properties of the C_{60}-f-SWNT composites electrophoretically deposited onto a nanostructured SnO_2 electrode.[24,25] A series of microscopic and photoelectrochemical studies on the deposited composite films has been performed to elucidate the relationship between the structures and the photoelectrochemical properties of the C_{60}-f-SWNT composites.

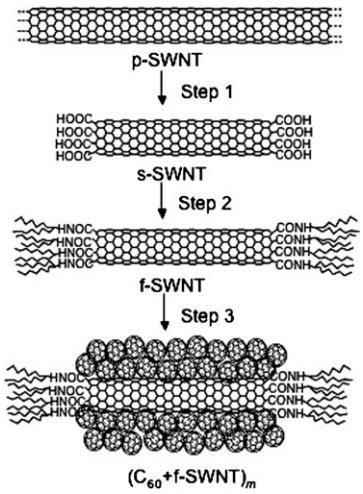

Scheme 1.

Results and Discussion

Preparation of functionalized SWNT: f-SWNT were prepared by purification and oxidation of p-SWNT (HiPco, purified grade) and subsequent reaction of s-SWNT with thionyl chloride and 8-aminopentadecane (see the Experimental Section).[2] f-SWNT are soluble in common organic solvents including *o*-dichlorobenzene, chloroform, THF, and toluene and show a solubility of up to $\approx 1.0\,g\,L^{-1}$ in ODCB after sonication for 30 min. The solution is stable for at least one month. Notably, the solubility of f-SWNT is remarkably improved relative to that of similar SWNT ($0.4\,g\,L^{-1}$ in ODCB)[5c] functionalized with long alkyl amines (i.e., octadecylamine) instead of the swallow-tailed secondary amines. The AFM image of f-SWNT (Figure 1a), which is obtained for the sample spin-coated on freshly cleaved mica from the ODCB solution of f-SWNT, discloses the short, thin rod-like structures attributed to the bundles of f-SWNT. The average diameter of isolated bundles of f-SWNT is determined to be 5.1 nm (see the Supporting Information, Figure S1). These results demonstrate that our strategy is useful for the solubilization of SWNT, which then allows π electron-rich compounds to interact with their sidewalls to make supramolecular complexes in organic solvents (vide infra).

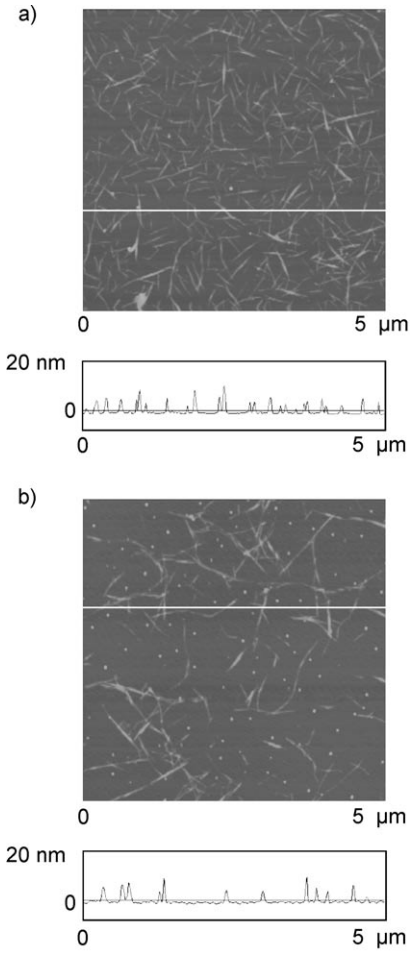

Figure 1. AFM images and section profiles of f-SWNT (Z range: 60 nm). The samples were prepared by spin-coating a solution of f-SWNT, in a) ODCB ($0.098\,g\,L^{-1}$) and b) ODCB/acetonitrile (1:3, v/v; $0.024\,g\,L^{-1}$), on freshly cleaved mica. The grey scale represents the height topography, with bright and dark representing the highest and lowest features, respectively.

Clusterization: UV-Vis-NIR absorption spectra of C_{60}, f-SWNT, and the composite were measured in ODCB and ODCB/acetonitrile mixtures (1:3, v/v). The absorption spectrum of f-SWNT (see the Supporting Information, Figure S2a) in ODCB ($0.024\,g\,L^{-1}$) shows characteristic peaks associated with transitions between symmetric van Hove singularities in the density of states for SWNT, which implies that the electronic structure of a SWNT is retained after the chemical modification.[2] The appearance of the moderately sharp peaks discloses that the f-SWNT is dispersed modestly in ODCB, since the sharpness of these peaks is widely considered to be a measure for the level of exfoliation of SWNT bundles. To examine the clusterization behavior of f-SWNT by lyophobic interaction, acetonitrile (poor solvent) was added rapidly to a solution of f-SWNT in ODCB (good solvent) ($0.098\,g\,L^{-1}$). The absorption spectrum of the resulting pale black, transparent solution in the ODCB/acetonitrile mixture (1:3, v/v; Figure S2b) is largely similar to that of f-SWNT in ODCB (Figure S2a) under the same concentration ($0.024\,g\,L^{-1}$). The similarity in the sharpness of the absorption peaks in the two spectra suggests that the size of the bundles is largely preserved after the injection of acetonitrile. However, there is a slight difference in the absorption intensity of f-SWNT in the mixed solvent relative to that in ODCB, which may be attributed to a small increase in the bundle size in the mixed solvent or difference in the solvent polarity or light scattering. Small vibration of the cuvette caused the precipitation of f-SWNT, making the solution transparent, thereby showing that the clusters of f-SWNT (denoted as $(\text{f-SWNT})_m$) are unstable in the mixed solvent (vide infra). The AFM image of f-SWNT (Figure 1b), which is obtained for the sample spin-coated on freshly cleaved mica from the ODCB/acetonitrile (1:3, v/v) solution of f-SWNT, also reveals the short, thin rod-like structures, but the average diameter (5.4 nm) of the isolated bundles is slightly larger than that from the ODCB solution (see Figure S1). Thus, we can conclude that the size of the bundles of f-SWNT in the mixed solvent is slightly larger than that in ODCB, owing to the lyophobic interaction with the mixed solvent.

In contrast, the clusterization behavior of C_{60} is different from that of f-SWNT. An ODCB/acetonitrile solution of C_{60} (1:3, v/v) was prepared by rapid injection of acetonitrile to an ODCB solution of C_{60} (0.56 mM). Compared with the absorption spectrum of C_{60} in ODCB (see the Supporting Information, Figure S3a), that in the mixed solvent (Figure S3b) exhibits broad absorption with a maximum at $\lambda = 520$ nm and the molar extinction coefficient in the mixed solvent is much larger than that in ODCB. The absorption behavior of C_{60} in the mixed solvent is attributed to the formation of stable C_{60} clusters (denoted as $(C_{60})_m$) by lyophobic interaction in the mixed solvent.[23] Dynamic light scattering (DLS) measurement of the cluster solution revealed that the size distribution of the cluster $(C_{60})_m$ is relatively narrow with an average diameter of 200 nm. Similar clusterization behavior of C_{60} is noted in toluene/acetonitrile mixture.[23]

The absorption spectrum of a mixture of C_{60} (0.56 mM, $0.40\,g\,L^{-1}$) and f-SWNT ($0.098\,g\,L^{-1}$) in ODCB, together with those of C_{60} and f-SWNT in ODCB is depicted in Figure 2. The absorption spectrum of the mixture in ODCB (Figure 2c) matches the sum of the absorption spectra of C_{60} and f-SWNT in ODCB (Figure 2d), implying that there is no significant interaction between C_{60} and f-SWNT in ODCB. The clusterization behavior of C_{60}-f-SWNT composite is also different from that of C_{60} and f-SWNT. The absorption spectrum of the mixture of C_{60} and f-SWNT in ODCB/acetonitrile (1:3, v/v) (Figure 3c)[26] shows structureless, broad absorption, which is different from those of C_{60} (Figure 3a) and f-SWNT (Figure 3b) in the same mixed solvents. Moreover, the absorption spectrum of the mixture of C_{60} and f-SWNT in the mixed solvent does not match the sum of the absorption spectra of f-SWNT and C_{60} in the same mixed solvents (Figure 3d). These results indicate that C_{60} molecules interact with f-SWNT to form the composite clusters of $(C_{60}+\text{f-SWNT})_m$ in the mixed solvent.

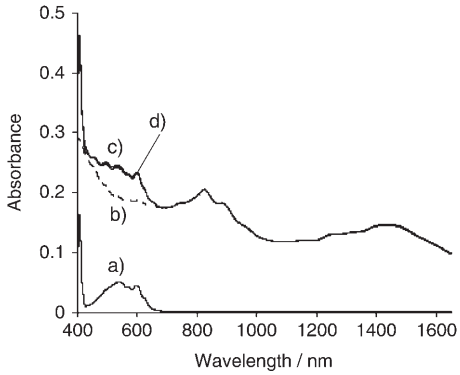

Figure 2. UV-Vis-NIR absorption spectra of a) C_{60} (0.56 mM, 0.40 g L^{-1}), b) f-SWNT (0.098 g L^{-1}), and c) a mixture of C_{60} (0.56 mM, 0.40 g L^{-1}) and f-SWNT (0.098 g L^{-1}) in ODCB. A cuvette (1 mm) was used for the measurements. d) Sum of spectra a) and b).

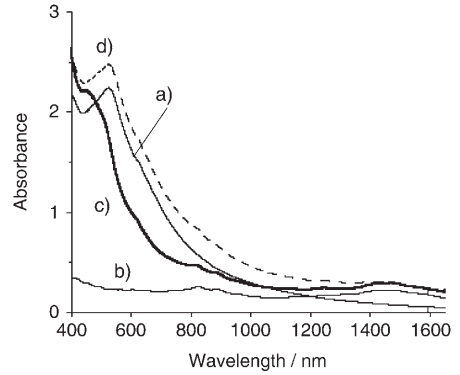

Figure 3. UV-Vis-NIR absorption spectra of a) C_{60} (0.070 mM, 0.050 g L^{-1}), b) f-SWNT (0.012 g L^{-1}), and c) a mixture of C_{60} (0.070 mM, 0.050 g L^{-1}) and f-SWNT (0.012 g L^{-1}) in ODCB/acetonitrile mixture (1:3, v/v). A cuvette (1 cm) was used for the measurements. d) Sum of spectra a) and b).

Field emission scanning electron microscopy (FE-SEM) measurements were performed to evaluate the shapes and morphology of C_{60}, f-SWNT, and the composite of C_{60} and f-SWNT in ODCB/acetonitrile mixture. The samples for the FE-SEM measurements were prepared by casting the ODCB/acetonitrile solution onto a glass plate. The FE-SEM image of $(C_{60})_m$ clusters discloses spherical particles with sizes between 150–350 nm (Figure 4a), which is consistent with the average diameter (200 nm) of $(C_{60})_m$ clusters obtained by the DLS measurement (vide supra). The FE-SEM image of f-SWNT reveals a spaghetti-like structure in which the fibrils are entangled (Figure 4b). Obviously, the observed fibrous structure results from the bundles of f-SWNT, as the size of individual f-SWNT (an average diameter of $\approx$1 nm) is beyond the instrument's resolution. On the other hand, the FE-SEM image of $(C_{60}+\text{f-SWNT})_m$ is classified into three groups (Figure 4c). The first area, Figure 4c (i), which is enlarged and rotated in Figure 4d, shows the entangled fibril-like structure as seen in the image of F-SWNT (Figure 4b). However, the average diameter of the fibrils is larger by 10–20 nm than that of f-SWNT in Figure 4b,[27] suggesting the interaction of the bundles of f-SWNT with C_{60} to yield the fibrils with the larger diameter (vide infra). The second area, Figure 4c(ii), displays a network structure in which spherical particles with diameters of 500–1000 nm are interconnected each other. The network structure suggests that C_{60} clusters are self-assembled with the bundles of f-SWNT to form larger clusters involving f-SWNT, resulting in the formation of the interconnected structure. In the third area, Figure 4c(iii), spherical particles exist with an average diameter of 200 nm, which agrees well with the size of the $(C_{60})_m$ clusters determined by using DLS and FE-SEM. Judging from the size and the shape, the spherical particles are assigned to $(C_{60})_m$. The formation of the $(C_{60})_m$ clusters is reasonable considering the high weight ratio of C_{60} vs. f-SWNT (4.1:1) in the mixed solution. Hereafter, the clusters observed in the areas Figure 4c(i)–(iii) are referred to clusters **I**, **II**, and **III**, respectively.[28]

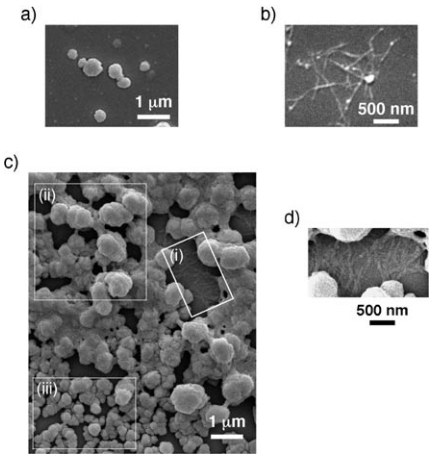

Figure 4. FE-SEM images of clusters of a) C_{60}, b) f-SWNT, and c) composites of f-SWNT and C_{60}. The samples were prepared by casting the solution of C_{60} (0.14 mM) and/or f-SWNT (0.024 g L^{-1}) in ODCB/acetonitrile (1:3, v/v) on a glass plate. The image c) is classified into three regions (i, ii, iii). d) Enlarged, rotated image of area (i) is shown for comparison.

Electrophoretic deposition: It is known that clusters of C_{60},[23–25] cup-stacked carbon nanostructures,[29] and SWNT[30,31] can be deposited electrophoretically onto electrodes by applying dc voltage to the electrode. In a similar manner, the clusters of C_{60}, f-SWNT, and the composites in the ODCB/acetonitrile mixture ($[C_{60}]=0.14$ mM, [f-SWNT] $=0.024$ g L^{-1}) were attached to nanostructured SnO_2 electrodes (denoted as FTO/SnO_2/$(C_{60})_m$, FTO/SnO_2/$(\text{f-SWNT})_m$, and FTO/SnO_2/$(C_{60}+\text{f-SWNT})_m$, in which FTO represents F-doped tin oxide), respectively. Under application of a high dc electric field (200 V for 120 s), the clusters of C_{60}, f-SWNT, and the composites, which are negatively charged in the mixed solvent, are driven toward the positively charged electrode (i.e., FTO/SnO_2). With increasing time of deposition, the FTO/SnO_2 electrode turns brown for $(C_{60})_m$ and $(C_{60}+\text{f-SWNT})_m$, or black for $(\text{f-SWNT})_m$ in color with simultaneous discoloration of the cluster solution. All of the electrophoretically deposited films are sufficiently

robust for the photoelectrochemical measurements. The change in absorbance of the electrophoretically deposited electrodes is monitored at $\lambda = 400$ nm with increasing time of deposition (see the Supporting Information, Figure S4). The time to reach a maximum absorbance becomes longer in the order of $(\text{f-SWNT})_m < (C_{60}+\text{f-SWNT})_m \sim (C_{60})_m$, showing the faster deposition of $(\text{f-SWNT})_m$ than that of $(C_{60})_m$. As we discuss later, the difference in the mobilities of the clusters affects the structures of the deposited composite film of C_{60} and f-SWNT. We used the electrodes prepared by the electrophoretic deposition of C_{60} and/or f-SWNT in ODCB/acetonitrile mixtures ($[C_{60}] = 0.14$ mM, [f-SWNT] = $0.024\ \text{g L}^{-1}$) for the duration time of 120 s, unless otherwise noted.

The UV-vis-NIR absorption spectra of the deposited films on nanostructured SnO_2 electrodes are shown in Figure 5. The absorption features of the deposited films are largely

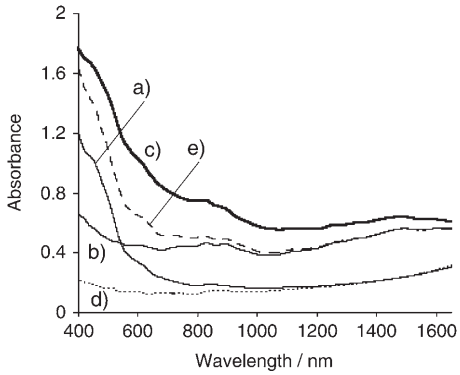

Figure 5. UV-Vis-NIR absorption spectra of a) FTO/SnO_2/$(C_{60})_m$, b) FTO/SnO_2/$(\text{f-SWNT})_m$, c) FTO/SnO_2/$(C_{60}+\text{f-SWNT})_m$, and d) FTO/SnO_2. e) Spectrum of a) plus b) minus d) is shown for comparison. The films were prepared from the corresponding solution with the concentrations of $[C_{60}] = 0.14$ mM and [f-SWNT] = $0.024\ \text{g L}^{-1}$ in ODCB/acetonitrile (1:3, v/v).

similar to those in the corresponding ODCB/acetonitrile solutions (Figure 3), showing that the clusters in the mixed solvent are successfully deposited onto the nanostructured SnO_2 electrodes without significant change in the cluster structures. In addition, the broad absorption of these films as well as the high molar absorptivity in the visible and near-IR regions makes these films suitable for harvesting the solar energy.

Resonant Raman spectroscopy is a valuable tool to characterize SWNT because it provides detailed information on the structure. Low-wavenumber phonon modes, radial breathing modes (RBMs), are very susceptible to the nanotube diameter and electronic states. Taking into account Kataura plot[32] with diameters of HiPco (0.8–1.3 nm),[8] one can monitor semiconducting and metallic SWNT with diameters of 0.8–1.0 and 1.0–1.3 nm, respectively, by an excitation energy of 1.96 eV ($\lambda_{ex} = 633$ nm). The resonant Raman spectra of FTO/SnO_2/$(C_{60})_m$, FTO/SnO_2/$(\text{f-SWNT})_m$, FTO/SnO_2/$(C_{60}+\text{f-SWNT})_m$, and f-SWNT cast on a glass plate from the ODCB solution were measured by means of laser excitation energy (1.96 eV, see Figure S5). The Raman spectrum of FTO/SnO_2/$(C_{60})_m$ exhibits several peaks ($\tilde{\nu} = 200$–$300\ \text{cm}^{-1}$) stemming from the vibration of C_{60} (Figure S5b).[33] The intensity of the Raman signals of FTO/SnO_2/$(C_{60})_m$, however, is much smaller than that of the FTO/SnO_2/$(\text{f-SWNT})_m$ (Figure S5c). On the other hand, it is well known that SWNT show characteristic peaks attributed to tangential mode (G-band) around $\tilde{\nu} = 1600\ \text{cm}^{-1}$ and disorder mode (D-band) around $\tilde{\nu} = 1350\ \text{cm}^{-1}$.[34] The ratio of the peak intensities (G/D ratio) reflects the relative amount of sp^3 carbon, and is used to determine the degree of functionalization in SWNT.[34] The G/D ratios of f-SWNT, FTO/SnO_2/$(\text{f-SWNT})_m$, and FTO/SnO_2/$(C_{60}+\text{f-SWNT})_m$ (Figure S5d) are virtually the same, which implies that the electronic structure of f-SWNT is preserved after the electrophoretic deposition of $(\text{f-SWNT})_m$ and $(C_{60}+\text{f-SWNT})_m$ onto FTO/SnO_2 electrodes. In addition, the positions and shapes of the peaks in RBM region are almost the same, indicating that the structure and composition of f-SWNT are also retained after the electrophoretic deposition.

FE-SEM was employed to evaluate the surface morphology of the films prepared by the electrophoretic deposition with the duration time of 120 seconds as shown in Figure 6.

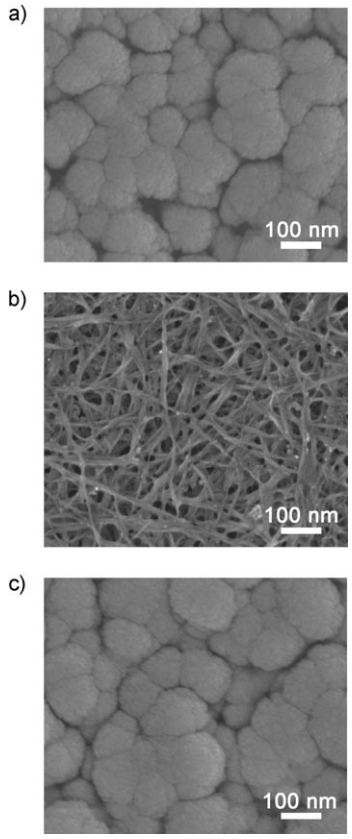

Figure 6. FE-SEM images of a) FTO/SnO_2/$(C_{60})_m$, b) FTO/SnO_2/$(\text{f-SWNT})_m$, and c) FTO/SnO_2/$(C_{60}+\text{f-SWNT})_m$ electrodes. The samples were prepared from their respective solutions ($[C_{60}] = 0.14$ mM, [f-SWNT] = $0.024\ \text{g L}^{-1}$) in ODCB/acetonitrile (1:3, v/v) by the electrophoretic deposition with a duration time of 120 s.

The FE-SEM image of the FTO/SnO_2/$(C_{60})_m$ electrode (Figure 6a) shows closely packed clusters with sizes of 100–200 nm, which are similar to that of $(C_{60})_m$ in the mixed solvent.[23–25] The FTO/SnO_2/(f-SWNT)$_m$ electrode reveals that the bundles of f-SWNT lie horizontally on the electrode surface and are entangled each other (Figure 6b). The spherical particles on the surface of the f-SWNT bundles may be metal particles that persist in the f-SWNT sample even after the purification procedure. The average diameter of the bundles is determined to be 12 nm (see Figure S6). It is noteworthy that the surface morphology of FTO/SnO_2/(C_{60}+f-SWNT)$_m$ (Figure 6c) is quite similar to that of FTO/SnO_2/$(C_{60})_m$ (Figure 6a). This observation manifests that the top layer of the (C_{60}+f-SWNT)$_m$ film consists of C_{60} clusters originating from the cluster **III** in Figure 4c. This result agrees well with the higher mobility of (f-SWNT)$_m$ than that of $(C_{60})_m$ during the electrophoretic deposition (Figure S4). We also performed AFM measurements of FTO/SnO_2/$(C_{60})_m$, FTO/SnO_2/(f-SWNT)$_m$, and FTO/SnO_2/(C_{60}+f-SWNT)$_m$ electrodes (see Figure S7). The AFM images of FTO/SnO_2/$(C_{60})_m$ (Figure S7a) and FTO/SnO_2/(C_{60}+f-SWNT)$_m$ (Figure S7c) exhibit the closely-packed $(C_{60})_m$ clusters with similar diameters of 100–200 nm, whereas that of FTO/SnO_2/(f-SWNT)$_m$ (Figure S7b) discloses the entangled, fibrous-shaped (f-SWNT)$_m$ clusters. The AFM images match well the corresponding SEM images.

To shed light on the inner topography of the (C_{60}+f-SWNT)$_m$ film on the FTO/SnO_2 electrode, we examined the change of the (C_{60}+f-SWNT)$_m$ films as a function of deposition time. Figure 7 shows the FE-SEM images of FTO/SnO_2/(C_{60}+f-SWNT)$_m$ electrodes obtained from the ODCB/acetonitrile solution (1:3, v/v) of C_{60} (0.14 mM) and f-SWNT (0.024 g L^{-1}) with the deposition time of 10, 20, 40, and 60 s. At the deposition time of 10 s, the FE-SEM image reveals entangled fibrous structures lying horizontally on the electrode surface (Figure 7a). The average diameter of the strings is estimated to be 18 nm (see Figure S8), which is evidently larger than that of the bundles (12 nm) of FTO/SnO_2/(f-SWNT)$_m$ without C_{60} (Figure 6b and Figure S6). This result is in accordance with the difference in the SEM images of (f-SWNT)$_m$ and cluster **I** (Figure 4b,d).[27,35] In addition, the FE-SEM image of FTO/SnO_2/(f-SWNT)$_m$ electrode at the deposition time of 10 s exhibits well-defined bundle structures (an average diameter of 12 nm), as seen in the FE-SEM image at the deposition time of 120 s (see Figure S9). Thus, we can conclude that the increase in the diameter of the strings in Figure 7a compared to that in Figure 6b is attributed to C_{60} molecules on the bundles of (f-SWNT)$_m$. In other words, when acetonitrile is injected into the ODCB solution of C_{60} and f-SWNT, some of C_{60} molecules interact with the sidewall of the bundles of f-SWNT by π-π and lyophobic interaction, leading to the arrangement of C_{60} molecules on the sidewall of the bundles of f-SWNT, as depicted in Scheme 1. Considering the difference (6 nm) in the average diameters of (f-SWNT)$_m$ and (C_{60}+f-SWNT)$_m$ on the electrodes, the thickness of the C_{60} layer is calculated to be ≈3 nm corresponding to three layers of C_{60}.

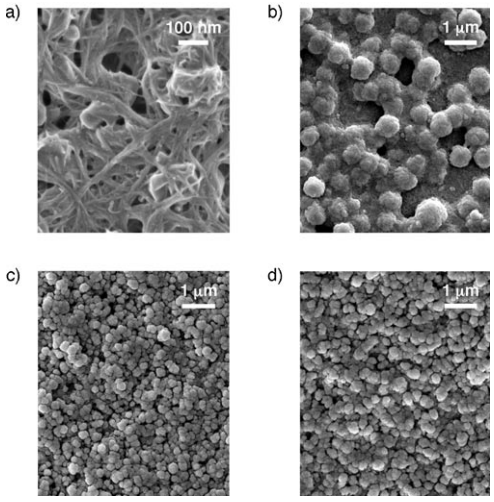

Figure 7. FE-SEM images of FTO/SnO_2/(C_{60}+f-SWNT)$_m$ electrodes obtained from the ODCB/acetonitrile solution (1:3, v/v) of C_{60} (0.14 mM) and f-SWNT (0.024 g L^{-1}) with the deposition time of a) 10 s, b) 20 s, c) 40 s, and d) 60 s.

At the deposition time of 20 s, the FE-SEM image of FTO/SnO_2/(C_{60}+f-SWNT)$_m$ electrode shows the structure composed of connected round-shaped, rugged particles with diameters of 500–1000 nm (Figure 7b). Taking into account the similar shape and size of the particles and cluster **II**, we assign the particles as cluster **II**, where small C_{60} clusters would be further self-assembled with f-SWNT to yield the large spherical clusters comprising of C_{60} and f-SWNT. The FE-SEM images of FTO/SnO_2/(C_{60}+f-SWNT)$_m$ electrodes at the deposition time of 40 and 60 s (Figure 7c,d) exhibit similar closely-packed particles with diameters of 150–300 nm, which are almost identical to the corresponding FE-SEM image at the deposition time of 120 s (Figure 6c). These results corroborate that clusters **I**, **II**, and **III** are sequentially deposited onto the FTO/SnO_2 electrode, depending on the difference in the mobilities under the application of dc voltage to the cluster solution, yielding the hierarchical film with the gradient composition along the direction of the film thickness.

Photoelectrochemical properties: Photoelectrochemical measurements were performed in deaerated acetonitrile containing LiI (0.5 M) and I_2 (0.01 M) with FTO/SnO_2/(C_{60}+f-SWNT)$_m$ as a working electrode, a platinum wire as a counter electrode, and I^-/I_3^- reference electrode. The FTO/SnO_2/(C_{60}+f-SWNT)$_m$ electrode was prepared from the cluster solution of (C_{60}+f-SWNT)$_m$ ([C_{60}] = 0.14 mM, [f-SWNT] = 0.024 g L^{-1}) in ODCB/acetonitrile (1:3, v/v). Figure 8a displays photocurrent response of the FTO/SnO_2/(C_{60}+f-SWNT)$_m$ electrode illuminated at an excitation wavelength of 400 nm (input power: 1.81 μW cm^{-2}) at +0.05 V vs. SCE. The photocurrent responses are prompt, steady, and reproducible during the repeated on/off cycles of the visible light illumination. Blank experiments of FTO/SnO_2

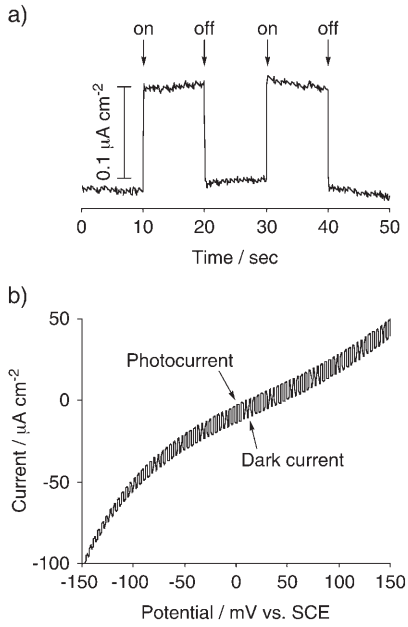

Figure 8. a) Photocurrent response of FTO/SnO_2/(C_{60}+f-SWNT)$_m$ illuminated at $\lambda = 400$ nm (1.81 μW cm^{-2}). Applied potential: +0.05 V vs. SCE; electrolyte: LiI (0.5 M) and I_2 (0.01 M) in acetonitrile. b) Current vs. applied potential curve for FTO/SnO_2/(C_{60}+f-SWNT)$_m$ device under illumination with white light ($\lambda > 380$ nm); input power: 78.8 mW cm^{-2}; electrolyte: LiI (0.5 M) and I_2 (0.01 M) in acetonitrile.

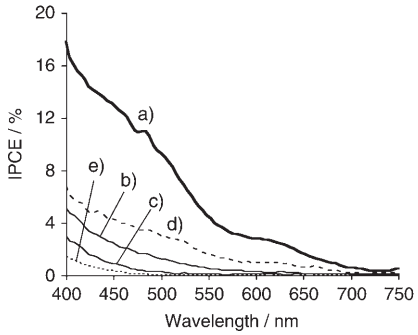

Figure 9. Photocurrent action spectra of a) FTO/SnO_2/(C_{60}+f-SWNT)$_m$, b) FTO/SnO_2/(C_{60})$_m$, c) FTO/SnO_2/(f-SWNT)$_m$, d) FTO/SnO_2/(f-SWNT)$_m$/(C_{60})$_m$, and e) FTO/SnO_2 electrodes. The electrodes were prepared from the ODCB/acetonitrile (1:3, v/v) solution of C_{60} and/or f-SWNT ([C_{60}] = 0.14 mM, [f-SWNT] = 0.024 g L^{-1}). Applied potential: +0.05 V vs. SCE; electrolyte: LiI (0.5 M) and I_2 (0.01 M) in acetonitrile.

electrode without the composite film exhibited much smaller photocurrent responses under the same conditions. These results confirm the role of the composite film toward harvesting light energy and generating electron flow from the electrolyte to the FTO/SnO_2 electrode through the film during the operation of the photoelectrochemical device. Figure 8b shows current-applied potential curve of the FTO/SnO_2/(C_{60}+f-SWNT)$_m$ system under white light illumination ($\lambda >$ 380 nm; input power: 78.8 mW cm^{-2}). With increasing positive bias up to 0.05 V vs. SCE, the photocurrent increases compared to the dark current. Increased charge separation and the facile transportation of charge carriers under positive bias are responsible for the enhanced photocurrent generation. As reported by Kamat et al. and our group,[23–25,30,31] FTO/SnO_2/(C_{60})$_m$ and FTO/SnO_2/(f-SWNT)$_m$ systems show similar photoelectrochemical behavior to that of the FTO/SnO_2/(C_{60}+f-SWNT)$_m$ system (vide infra).

To evaluate the photoelectrochemical response of the FTO/SnO_2/(C_{60}+f-SWNT)$_m$ system, we examined the wavelength dependence of the incident photon-to-photocurrent efficiency (IPCE) of the film on FTO/SnO_2. The IPCE values are calculated by normalizing the photocurrent densities for incident light energy and intensity and by use of the expression in Equation (1):

$$\text{IPCE}\ (\%) = 100 \times 1240 \times i/(W_{\text{in}} \times \lambda) \qquad (1)$$

in which i is the photocurrent density (A cm^{-2}), W_{in} is the incident light intensity (W cm^{-2}), and λ is the excitation wavelength (nm). Figure 9a illustrates the photocurrent action spectrum of the FTO/SnO_2/(C_{60}+f-SWNT)$_m$ system. The maximum IPCE value reaches up to 18% at 400 nm under an applied potential of 0.05 V vs. SCE. It should be noted here that the IPCE value of the FTO/SnO_2/(C_{60}+f-SWNT)$_m$ system monotonically decreases with increasing the wavelength to reach almost zero at $\lambda = 730$ nm, which does not match the absorption feature of the FTO/SnO_2/(C_{60}+f-SWNT)$_m$ electrode (Figure 5c). Namely, the FTO/SnO_2/(C_{60}+f-SWNT)$_m$ electrode exhibits significant absorbance at $\lambda = 700$–1600 nm, which mainly results from the absorption of f-SWNT and light scattering. These results suggest that the absorption of visible light (400–700 nm) by C_{60} molecules is responsible for the photocurrent generation and the contribution by the excitation of f-SWNT is minor.

The photocurrent action spectrum of the FTO/SnO_2/(C_{60}+f-SWNT)$_m$ system is also compared to those of the FTO/SnO_2/(C_{60})$_m$, FTO/SnO_2/(f-SWNT)$_m$, and FTO/SnO_2 to gain deep insight into the photocurrent generation (Figure 9). The IPCE values of FTO/SnO_2/(C_{60}+f-SWNT)$_m$ (Figure 9a) system are 3–5 times as large as those of the FTO/SnO_2/(C_{60})$_m$ (Figure 9b) and FTO/SnO_2/(f-SWNT)$_m$ (Figure 9c). In addition, the IPCE values of the FTO/SnO_2/(C_{60}+f-SWNT)$_m$ system are still much larger than those of the FTO/SnO_2/(f-SWNT)$_m$/(C_{60})$_m$ (Figure 9d), in which the FTO/SnO_2/(f-SWNT)$_m$ electrode is further modified with (C_{60})$_m$ electrophoretically by using the cluster solution ([C_{60}] = 0.14 mM in ODCB/acetonitrile). Thus, the complex formation of C_{60} and f-SWNT in the mixed solvent by the lyophobic and π–π interactions is essential for the efficient photocurrent generation. It should be emphasized here that the observed maximum IPCE value of 18% in FTO/SnO_2/(C_{60}+f-SWNT)$_m$ system is the highest among the carbon nanotube-based photoelectrochemical devices (up to 9.3%) in which the carbon nanotubes are deposited onto electrodes electrophoretically,[30] electrostatically[36] or covalently.[37]

To examine the relationship between the gradient composition of the composite films along the direction of the film thickness and the photocurrent generation, photocurrent action spectra of the FTO/SnO_2/(C_{60}+f-SWNT)$_m$ system

(Figure 10) were measured by using the FTO/SnO_2/(C_{60}+f-SWNT)$_m$ electrodes prepared with different deposition time (i.e., 10, 20, 40, 120 s). The UV-vis absorption spectra

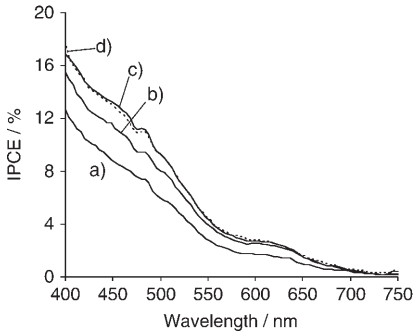

Figure 10. Photocurrent action spectra of FTO/SnO_2/(C_{60}+f-SWNT)$_m$ electrodes prepared by the electrophoretic method with deposition time of a) 10 s, b) 20 s, c) 40 s, and d) 120 s; [C_{60}] = 0.14 mM, [f-SWNT] = 0.024 g L^{-1} in ODCB/acetonitrile (1:3, v/v); applied potential: +0.05 V vs. SCE; electrolyte: LiI (0.5 M) and I_2 (0.01 M) in acetonitrile.

of the FTO/SnO_2/(C_{60}+f-SWNT)$_m$ electrodes (see the Supporting Information, Figure S10) are also monitored to compare the corresponding FE-SEM images (Figure 7a–c and Figure 6c) and the photocurrent action spectra. All the electrodes exhibit similar structureless absorption and the absorbance gradually increases with increasing the deposition time. The overall photocurrent action spectra of the FTO/SnO_2/(C_{60}+f-SWNT)$_m$ system parallel the broad absorption spectral features. Notably, with increasing the deposition time (0–40 s), the IPCE values increase and level off at the deposition time of 40–120 s. Considering the exclusive deposition of cluster **I**, the bundles of f-SWNT covered with C_{60} molecules, at the deposition time of 10 s and the corresponding large IPCE value (12.5% at $\lambda = 400$ nm), the film of cluster **I** without clusters **II** and **III** has a large impact on the photocurrent generation. The aligned C_{60} molecules on the bundles of f-SWNT are responsible for the efficient photocurrent generation. The gradual increase in the IPCE values with the deposition time of 20 and 40 s relative to that with the deposition time of 10 s reveals that the cluster **II** (large-sized C_{60} cluster including f-SWNT) and cluster **III** (middle-sized C_{60} cluster) also make contribution to the photocurrent generation.

Photocurrent generation mechanism: On the basis of the previous studies on similar photochemical systems consisting of C_{60}[23] or f-SWNT[30,31] as well as the film structure and the photoelectrochemical properties of the present system, we propose photocurrent generation mechanism as shown in Schemes 2,3, and S1 (see the Supporting Information). As a representative example, (8,6) SWNT, which is the highest distribution of (*n*,*m*) species ((*n*,*m*) determines the diameter and direction of the tube's rolling) in the present p-SWNT, is given in the schemes.[31,38] Although the direct injection from the excited states of f-SWNT to the conduction band

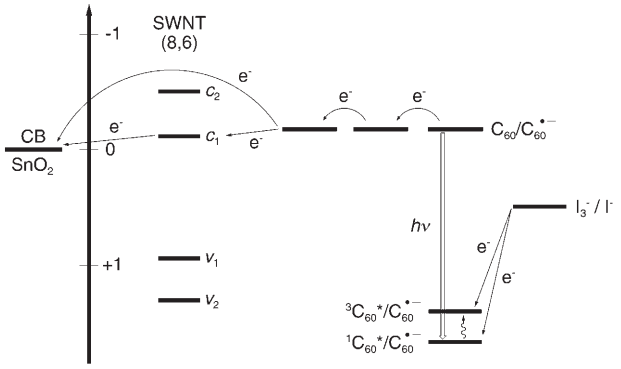

Scheme 2.

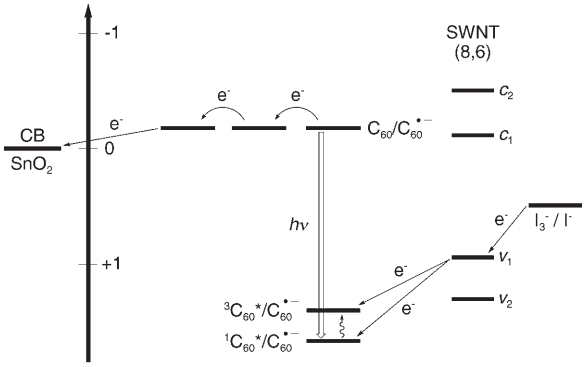

Scheme 3.

(CB) of SnO_2 is possible (Scheme S1), its contribution in the present system should be minor according to the photocurrent action spectrum of FTO/SnO_2/(f-SWNT)$_m$ system (Figure 9c).

Scheme 2 illustrates a plausible photocurrent generation pathway, in which photoinduced ET between iodide ion ($I_3^-/I^- = 0.5$ V vs. NHE)[23] and the excited states of C_{60} ($^1C_{60}^* = 1.7$ V vs. NHE; $^3C_{60}^* = 1.4$ V vs. NHE)[23] is the primary step in the photocurrent generation. The reduced C_{60} ($C_{60}/C_{60}^{\bullet-} = -0.2$ V vs. NHE)[23] injects an electron into the CB of SnO_2 ($E_{CB} = 0$ V vs. NHE) through electron hopping between C_{60} molecules. ET from the C_{60} molecules of clusters **I**, **II**, and **III** to the f-SWNT ($c_1 = -0.094$ V vs. NHE) may also occur to transport the electron to the SnO_2 electrode through the network of the f-SWNT. The electron transferred to the SnO_2 electrode is driven to the counter electrode through an external circuit to regenerate the redox couple. The highly aligned structure of C_{60} molecules on the f-SWNT sidewalls and the high electron transport capability of f-SWNT may facilitate the electron flow, leading to the efficient photocurrent generation in the present system. In addition to the mechanisms in Scheme 2, direct CS between C_{60} and f-SWNT in clusters **I** and **II** for the photocurrent generation is energetically possible (Scheme 3). Namely, initial ET takes place from v_1 (or v_2) of f-SWNT (0.96 V vs. NHE) to the C_{60} excited states. Then, subsequent ET from the reduced C_{60} to the CB of the SnO_2 electrode

and from I^- to v_1 (or v_2) of f-SWNT occurs, resulting in the photocurrent generation. We tried to measure the transient absorption spectrum of $(C_{60}+\text{f-SWNT})_m$ cluster in the ODCB/acetonitrile mixture, but the attempt was unsuccessful, owing to the instability of the clusters under the laser-irradiation conditions. The preliminary transient absorption measurements using the FTO/SnO_2/$(C_{60}+\text{f-SWNT})_m$ electrode did not exhibit the fingerprint of C_{60} radical anion at $\lambda = 1000$–1100 nm, which indicated no occurrence of direct CS between C_{60} and f-SWNT. Thus, the photocurrent generation mechanism in Scheme 3 may be ruled out.

Conclusion

We have successfully developed the novel strategy for the arrangement of C_{60} molecules on the external surface of SWNT. First, acid treatment cuts pristine SWNT to yield shortened SWNT with carboxylic groups at the open ends and defect sites. Then, the shortened SWNT is functionalized with sterically bulky amine to yield highly soluble, functionalized SWNT (f-SWNT) in organic solvents. Finally, poor solvent (i.e., acetonitrile) is rapidly injected into a mixture of C_{60} and f-SWNT in good solvent (*o*-dichlorobenzene), resulting in formation of the composite clusters of C_{60} and f-SWNT. The lyophobic interaction between C_{60}-f-SWNT and the mixed solvent as well as the π–π interaction between C_{60} molecules and between C_{60} and f-SWNT was found to be responsible for the desirable arrangement of C_{60} molecules on the external surface of SWNT in the mixed solvent. The electrophoretic deposition of the composites onto a nanostructured SnO_2 electrode gradually yielded the hierarchical film with gradient composition depending on the difference in the mobilities of C_{60} and f-SWNT during the electrophoretic process. The composite film exhibited an incident photon-to-photocurrent efficiency as high as 18% at $\lambda = 400$ nm under an applied potential of 0.05 V vs. SCE. The photocurrent generation efficiency is the highest value among carbon nanotube-based photoelectrochemical devices in which carbon nanotubes are deposited onto electrodes electrophoretically, electrostatically or covalently.[30,36,37] The highly aligned structure of C_{60} molecules on f-SWNT can rationalize the efficient photocurrent generation. Thus, the results obtained here will provide valuable information on the design of carbon nanotube-based molecular devices.

Experimental Section

General procedures: UV-Vis-near infrared (NIR) spectra of solutions and films were measured by using a Perkin–Elmer Lambda 900 UV/vis/NIR spectrometer. Resonance Raman spectra were recorded by using a Horiba JobinYvon LabRAM HR-800 equipped with a 1.96 eV (633 nm) laser. Field emission scanning electron microscopy (FE-SEM) observation was carried out by using a JEOL JSM-6500FE, JSM-7500F, and a Hitachi S-4700. For preparation of the cluster samples, a mixture of ODCB/acetonitrile containing f-SWNT and/or C_{60} was cast on glass plates and the solvent was evaporated. The samples in Figures 4, 6a,c and 7b–d were coated with Pt by using a JEOL JFC-1600 auto fine coater before the measurements. Atomic force microscopy (AFM) images of SWNT samples were obtained by means of a Digital Instruments Nanoscope III in the tapping mode. A solution containing f-SWNT and/or C_{60} was spin-coated on freshly cleaved mica at a rotation speed of 500 rpm. Dynamic light scattering (DLS) measurements of the cluster solutions were performed by using a Horiba LB550 particle size analyzer. s-SWNT was prepared by using HiPco SWNT (Carbon Nanotechnologies, Inc.) as published elsewhere.[2] 8-Aminopentadecane was synthesized according to the literature.[39] C_{60} (99.98%) was obtained from MTR Ltd. An optically transparent fluorine-doped tin oxide electrode (denoted as FTO; Asahi Glass Inc.) was washed by sonication in 2-propanol and cleaned in an O_3 atmosphere in advance. A 15% SnO_2 colloidal solution (particle size = 15 nm; Chemat Technology, Inc.) was deposited on the FTO electrode using the doctor blade technique.[23g,25e–g] The electrode was annealed at 673 K (denoted as FTO/SnO_2) to yield 1.3-μm-thick SnO_2 film. All other chemicals were purchased from commercial sources and used without further purification.

Synthesis of f-SWNT: s-SWNT (45 mg) was dispersed in thionyl chloride (10 mL) and stirred vigorously at 70°C for 1 day under Ar. The excess thionyl chloride was removed by distillation under reduced pressure. To the remaining black solid was added 8-aminopentadecane (5 mL) in the glovebox and the mixture was stirred at 100°C for 5 days. Cooled to room temperature, the reaction mixture was diluted by ethanol and filtered through a 0.22 μm polycarbonate membrane filter. The resulting black residue was washed with ethanol, acetone, and hexane repeatedly. Reprecipitation from ODCB/methanol and subsequent ODCB/acetone and finally drying at 60°C for 9 h gave the functionalized SWNT (f-SWNT, 41 mg).

Preparation of cluster solutions and films: The cluster solutions of f-SWNT (0.024 $g\,L^{-1}$) and/or C_{60} (0.14 mM) were prepared in a 1 cm cuvette by injecting acetonitrile (1.2 mL) into a solution of f-SWNT (0.098 $g\,L^{-1}$) and/or C_{60} (0.56 mM) in ODCB (0.4 mL) (ODCB/acetonitrile = 1:3, v/v).[23–25] Two electrodes (i.e., FTO and FTO/SnO_2) were inserted into the cuvette with keeping at a distance of 6.0 mm by a Teflon spacer. A dc voltage (200 V) was applied for 2 min between these two electrodes using a power supply (ATTA model AE-8750). The deposition of the film could be visibly confirmed as the suspension became colorless with the simultaneous colorization of the FTO/SnO_2 electrode. After the deposition, the deposited film was dried immediately with a hair dryer.

Photoelectrochemical measurements: All electrochemical measurements were carried out in a standard three-electrode system using an ALS 630a electrochemical analyzer.[23f,25e–g] The deposited film as a working electrode was immersed into the electrolyte solution containing LiI (0.5 M) and I_2 (0.01 M) in acetonitrile. A Pt wire covered with a glass Luggin capillary, whose tip was located near the working electrode, was used as a quasi-reference electrode, whereas a Pt coil was employed as a counter electrode. The potential measured was converted to the saturated calomel electrode (SCE) scale by adding +0.05 V. The stability of the reference electrode potential was confirmed under the experimental conditions. A 500 W xenon lamp (XB-50101 AAA; Ushio, Japan) was used as a light source. Potential versus current characteristics were measured with controlled-potential scan (1 $mV\,s^{-1}$) under 0.5 Hz chopped white light ($\lambda > 380$ nm; input power, 78.8 $mW\,cm^{-2}$). The modified area of the working electrode (0.20 cm^2) was illuminated from the backside by monochromatic light through a monochromator (MC-10N; Ritsu, Japan). The light intensity was monitored by an optical power meter (ML9002 A; Anritsu, Japan) and corrected.

Acknowledgement

H. I. thanks Grand-in-Aid from MEXT, Japan (Priority Area of Molecular Theory for Real Systems (No. 19029020) for financial support. T. U. acknowledges the support by the Global COE Program "Integrated Materials Science" (B-09). We also thank Ms. Heli Lehtivuori, Prof. Nicolai V. Tkachenko and Prof. Helge Lemmetyinen (Tampere Univ.) for the

measurements of transient absorption spectra, Prof. Naoki Komatsu and Mr. Takanori Shimawaki (Shiga Univ. of Medical Science) for the resonant Raman spectroscopy measurements, and Prof. Susumu Yoshikawa and Prof. Takashi Sagawa (Kyoto Univ.) for the FE-SEM measurements.

[1] a) S. Niyogi, M. A. Hamon, H. Hu, B. Zhao, P. Bhowmik, R. Sen, M. E. Itkis, R. C. Haddon, *Acc. Chem. Res.* **2002**, *35*, 1105; b) Y.-P. Sun, K. Fu, Y. Lin, W. Huang, *Acc. Chem. Res.* **2002**, *35*, 1096; c) E. Katz, I. Willner, *ChemPhysChem* **2004**, *5*, 1084; d) C. A. Dyke, J. M. Tour, *J. Phys. Chem. A* **2004**, *108*, 11151; e) C. A. Dyke, J. M. Tour, *Chem. Eur. J.* **2004**, *10*, 812; f) D. M. Guldi, G. M. A. Rahman, F. Zerbetto, M. Prato, *Acc. Chem. Res.* **2005**, *38*, 871; g) D. Tasis, N. Tagmatarchis, A. Blamco, M. Prato, *Chem. Rev.* **2006**, *106*, 1105.

[2] a) J. Chen, M. A. Hamon, H. Hu, Y. Chen, M. A. Rao, P. C. Eklund, R. C. Haddon, *Science* **1998**, *282*, 95; b) Y.-P. Sun, W. Huang, Y. Lin, K. Fu, A. Kitaygorodskiy, L. A. Riddle, Y. J. Yu, D. L. Carroll, *Chem. Mater.* **2001**, *13*, 2864; c) Y. Lian, Y. Maeda, T. Wakahara, T. Akasaka, S. Kazaoui, N. Minami, N. Choi, H. Tokumoto, *J. Phys. Chem. B* **2003**, *107*, 12082; d) M. Alvaro, P. Atienzar, P. de la Cruz, J. L. Delgado, H. Garcia, F. Langa, *Chem. Phys. Lett.* **2004**, *386*, 342; e) H. Jia, Y. Lian, M. O. Ishitsuka, T. Nakahodo, Y. Maeda, T. Tsuchiya, T. Wakahara, T. Akasaka, *Sci. Technol. Adv. Mater.* **2005**, *6*, 571; f) M. A. Herranz, N. Martin, S. Campidelli, M. Prato, G. Brehm, D. M. Guldi, *Angew. Chem.* **2006**, *118*, 4590; *Angew. Chem. Int. Ed.* **2006**, *45*, 4478.

[3] a) J. L. Bahr, J. Yang, D. V. Kosynkin, M. J. Bronikowski, R. E. Smalley, J. M. Tour, *J. Am. Chem. Soc.* **2001**, *123*, 6536; b) J. L. Bahr, J. M. Tour, *Chem. Mater.* **2001**, *13*, 3823; c) J. L. Bahr, J. M. Tour, *J. Mater. Chem.* **2002**, *12*, 1952; d) M. S. Strano, C. A. Dyke, M. L. Usrey, P. W. Barone, M. J. Allen, H. Shan, C. Kittrell, R. H. Hauge, J. M. Tour, R. E. Smalley, *Science* **2003**, *301*, 1519; e) J. J. Stephenson, J. L. Hudson, S. Azad, J. M. Tour, *Chem. Mater.* **2006**, *18*, 374.

[4] a) V. Georgakilas, K. Kordatos, M. Prato, D. M. Guldi, M. Holzinger, A. Hirsch, *J. Am. Chem. Soc.* **2002**, *124*, 760; b) V. Georgakilas, D. Voulgaris, E. Vazquez, M. Prato, D. M. Guldi, A. Kukovecz, H. Kuzmany, *J. Am. Chem. Soc.* **2002**, *124*, 14318; c) D. M. Guldi, M. Marcaccio, D. Paolucci, F. Paolucci, N. Tagmatarchis, D. Tasis, E. Vazquez, M. Prato, *Angew. Chem.* **2003**, *115*, 4338; *Angew. Chem. Int. Ed.* **2003**, *42*, 4206; d) M. Melle-Franco, M. Marcaccio, D. Paolucci, F. Paolucci, V. Georgakilas, D. M. Guldi, M. Prato, F. Zerbetto, *J. Am. Chem. Soc.* **2004**, *126*, 1646; e) N. Tagmatarchis, M. Prato, *J. Mater. Chem.* **2004**, *14*, 437.

[5] a) K. S. Coleman, S. R. Bailey, S. Fogden, M. L. H. Green, *J. Am. Chem. Soc.* **2003**, *125*, 8722; b) K. A. Worsley, K. R. Moonoosawmy, P. Kruse, *Nano Lett.* **2004**, *4*, 1541; c) T. Umeyama, N. Tezuka, M. Fujita, Y. Matano, N. Takeda, K. Murakoshi, K. Yoshida, S. Isoda, H. Imahori, *J. Phys. Chem. C* **2007**, *111*, 9734.

[6] a) J. L. Delgado, P. Cruz, F. Langa, A. Urbina, J. Casado, J. T. L. Navarrete, *Chem. Commun.* **2004**, 1734; b) M. Alvaro, P. Atienzar, P. de la Cruz, J. L. Delgado, H. Garcia, F. Langa, *J. Phys. Chem. B* **2004**, *108*, 12691; c) M. Alvaro, P. Atienzar, P. de la Cruz, J. L. Delgado, V. Troiani, H. Garcia, F. Langa, A. Palkar, L. Echegoyen, *J. Am. Chem. Soc.* **2006**, *128*, 6626.

[7] a) Y. Wang, Z. Iqbal, S. Mitra, *Carbon* **2005**, *43*, 1015; b) K. Kubota, M. Sano, T. Masuko, *Jpn. J. Appl. Phys.* **2005**, *44*, 465; c) Y. Wang, Z. Iqbal, S. Mitra, *J. Am. Chem. Soc.* **2006**, *128*, 95; d) J. Li, H. Grennberg, *Chem. Eur. J.* **2006**, *12*, 3869; e) Y. Wang, Z. Iqbal, S. Mitra, *Carbon* **2006**, *44*, 2804.

[8] a) J. Liu, A. G. Rinzler, H. Dai, J. H. Hafner, R. K. Bradley, P. J. Boul, A. Lu, T. Iverson, K. Shelimov, C. B. Huffman, F. Rodriguez-Macias, Y.-S. Shon, T. R. Lee, D. T. Colbert, R. E. Smalley, *Science* **1998**, *280*, 1253; b) V. C. Moore, M. S. Strano, E. H. Haroz, R. H. Hauge, R. E. Smalley, J. Schmidt, Y. Talmon, *Nano Lett.* **2003**, *3*, 1379; c) M. F. Islam, E. Rojas, D. M. Bergey, A. T. Johnson, A. G. Yodh, *Nano Lett.* **2003**, *3*, 269; d) M. J. O'Connell, S. M. Bachilo, C. B. Huffman, V. C. Moore, M. S. Strano, E. H. Haroz, K. L. Rialon, P. J. Boul, W. H. Noo, C. Kittrell, J. Ma, R. H. Hauge, R. B. Weisman, R. E. Smalley, *Science* **2002**, *297*, 593; e) S. M. Bachilo, M. S. Strano, C. Kittrell, R. H. Hauge, R. E. Smalley, R. B. Weisman, *Science* **2002**, *298*, 2361.

[9] a) N. Nakashima, Y. Tomonari, H. Murakami, *Chem. Lett.* **2002**, *31*, 638; b) D. M. Guldi, G. M. A. Rahaman, N. Jux, N. Tagmatarchis, M. Prato, *Angew. Chem.* **2004**, *116*, 5642; *Angew. Chem. Int. Ed.* **2004**, *43*, 5526; c) T. Ogoshi, Y. Takashima, H. Yamaguchi, A. Harada, *J. Am. Chem. Soc.* **2007**, *129*, 4878.

[10] a) M. J. O'Connell, P. Boul, L. M. Ericson, C. Huffman, Y. Wang, E. Haroz, C. Kuper, J. Tour, K. D. Ausman, R. E. Smalley, *Chem. Phys. Lett.* **2001**, *342*, 265; b) M. Zheng, A. Jagota, E. D. Semke, B. A. Diner, R. S. Mclean, S. R. Lustig, R. E. Richardson, N. G. Tassi, *Nat. Mater.* **2003**, *2*, 338; c) A. Star, D. W. Steuerman, J. R. Heath, J. F. Stoddart, *Angew. Chem.* **2002**, *114*, 2618; *Angew. Chem. Int. Ed.* **2002**, *41*, 2508; d) M. Numata, M. Asai, K. Kaneko, A.-H. Bae, T. Hasegawa, K. Sakurai, S. Shinkai, *J. Am. Chem. Soc.* **2005**, *127*, 5875.

[11] a) R. J. Chen, Y. Zhang, D. Wang, H. Dai, *J. Am. Chem. Soc.* **2001**, *123*, 3838; b) F. J. Gomez, R. J. Chen, D. Wang, R. M. Waymouth, H. Dai, *Chem. Commun.* **2003**, 190; c) D. M. Guldi, E. Menna, M. Maggini, M. Marcaccio, D. Paolucci, F. Paolucci, S. Campidelli, M. Prato, G. M. A. Rahman, S. Schergna, *Chem. Eur. J.* **2006**, *12*, 3975; d) R. Chitta, A. S. D. Sandanayaka, A. L. Schumacher, L. D'Souza, Y. Araki, O. Ito, F. D'Souza, *J. Phys. Chem. C* **2007**, *111*, 6947.

[12] a) H. Murakami, T. Nomura, N. Nakashima, *Chem. Phys. Lett.* **2003**, *378*, 481; b) H. Li, B. Zhou, Y. Lin, L. Gu, W. Wang, K. A. S. Fernando, S. Kumar, L. F. Allard, Y.-P. Sun, *J. Am. Chem. Soc.* **2004**, *126*, 1014; c) T. Hasobe, S. Fukuzumi, P. V. Kamat, *J. Am. Chem. Soc.* **2005**, *127*, 11884; d) F. Cheng, A. Adronov, *Chem. Eur. J.* **2006**, *12*, 5053; e) F. Y. Chen, S. Zhang, A. Adronov, L. Echegoyen, F. Diederich, *Chem. Eur. J.* **2006**, *12*, 6062; f) F. Langa, M. J. Gomez-Escalonilla, P. de la Cruz, *J. Porphyrins Phthalocyanines* **2007**, *11*, 348.

[13] a) S. A. Curran, P. M. Ajayan, W. J. Blau, D. L. Carroll, J. N. Coleman, A. B. Dalton, A. P. Davey, A. Drury, B. McCarthy, S. Maier, A. Strevens, *Adv. Mater.* **1998**, *10*, 1091; b) D. W. Steuerman, A. Star, R. Narizzano, H. Choi, R. S. Ries, C. Nicolini, J. F. Stoddart, J. R. Heath, *J. Phys. Chem. B* **2002**, *106*, 3124; c) J. Chen, H. Liu, W. A. Weimer, M. D. Halls, D. H. Ealdeck, G. C. Walker, *J. Am. Chem. Soc.* **2002**, *124*, 9034; d) A. Star, Y. Liu, K. Grant, L. Ridvan, J. F. Stoddart, D. W. Steuerman, M. R. Diehl, A. Boukai, J. R. Heath, *Macromolecules* **2003**, *36*, 553; e) A. Ikeda, K. Nobusawa, T. Hamano, J.-i. Kikuchi, *Org. Lett.* **2006**, *8*, 5489; f) T. Umeyama, N. Kadota, N. Tezuka, Y. Matano, H. Imahori, *Chem. Phys. Lett.* **2007**, *444*, 263.

[14] a) H. Ago, K. Petritsch, M. S. P. Shaffer, A. H. Windle, R. H. Friend, *Adv. Mater.* **1999**, *11*, 1281; b) A. Star, J. F. Stoddart, D. Steuerman, M. Diehl, A. Boukai, E. W. Wong, X. Yang, S.-W. Chung, H. Choi, J. R. Heath, *Angew. Chem.* **2001**, *113*, 1771; *Angew. Chem. Int. Ed.* **2001**, *40*, 1721; c) S. Bhattacharyya, E. Kymakis, G. A. J. Amaratunga, *Chem. Mater.* **2004**, *16*, 4819; d) T. Hasobe, S. Fukuzumi, P. V. Kamat, *J. Phys. Chem. B* **2006**, *110*, 25477.

[15] a) M. S. Dresselhaus, G. Dresselhaus, P. C. Eklund, *Science of Fullerenes and Carbon Nanotubes*, Academic Press, San Diego, **1996**; b) *Fullerenes* (Eds.: K. M. Kadish, R. S. Ruoff), Wiley, New York, **2000**; c) S. Reich, C. Thomsen, J. Maultzsch, *Carbon Nanotubes*, Wiley-VCH, Weinheim, **2004**; d) *Applied Physics of Carbon Nanotubes* (Eds.: S. V. Rotkin, S. Subramoney) Springer, Berlin, **2005**; e) *Organic Photovoltaics* (Eds.: C. Brabec, V. Dyakonov, J. Parisi, N. S. Sariciftci), Springer, Berlin, **2003**.

[16] a) D. M. Guldi, *J. Phys. Chem. B* **2005**, *109*, 11432; b) P. V. Kamat, *J. Phys. Chem. C* **2007**, *111*, 2834.

[17] a) H. Imahori, Y. Sakata, *Adv. Mater.* **1997**, *9*, 537; b) H. Imahori, Y. Sakata, *Eur. J. Org. Chem.* **1999**, 2445; c) H. Imahori, *Org. Biomol. Chem.* **2004**, *2*, 1425; d) H. Imahori, *J. Phys. Chem. B* **2004**, *108*, 6130; e) H. Imahori, S. Fukuzumi, *Adv. Funct. Mater.* **2004**, *14*, 525; f) H. Imahori, *Bull. Chem. Soc. Jpn.* **2007**, *80*, 621.

[18] a) B. W. Smith, M. Monthioux, D. E. Luzzi, *Nature* **1998**, *396*, 323; b) H. Kataura, Y. Maniwa, M. Abe, A. Fujiwara, T. Kodama, K. Ki-

kuchi, H. Imahori, Y. Misaki, S. Suzuki, Y. Achiba, *Appl. Phys. A* **2002**, *74*, 349; c) D. A. Britz, A. N. Khlobystov, J. Wang, A. S. O'Neil, M. Poliakoff, A. Ardavan, G. A. D. Briggs, *Chem. Commun.* **2004**, 176; d) A. N. Khlobystov, D. A. Britz, G. A. D. Briggs, *Acc. Chem. Res.* **2005**, *38*, 901.

[19] There are a few reports on C_{60}-SWNT composite system other than bucky-peapods. a) Y. Takaguchi, M. Tamura, Y. Sako, Y. Yanagimoto, S. Tsuboi, T. Uchida, K. Shimamura, S. Kimura, T. Wakahara, Y. Maeda, T. Akasaka, *Chem. Lett.* **2005**, *34*, 1608; b) D. M. Guldi, E. Menna, M. Maggini, M. Marcaccio, D. Paolucci, F. Paolucci, S. Campidelli, M. Prato, G. M. A. Rahman, S. Schergna, *Chem. Eur. J.* **2006**, *12*, 3975; c) A. G. Nasibulin, P. V. Pikhitsa, H. Jiang, D. P. Brown, A. V. Krasheninnikov, A. S. Anisimov, P. Queipo, A. Moisala, D. Gonzalez, G. Lientschnig, A. Hassanien, S. D. Shandakov, G. Lolli, D. E. Resasco, M. Choi, D. Tománek, E. I. Kauppinen, *Nat. Nanotechnol.* **2007**, *2*, 156; d) J. L. Delgado, P. Cruz, A. Urbina, J. T. L. Navarrete, J. Casado, F. Langa, *Carbon* **2007**, *45*, 2250.

[20] a) A. D. Pasquier, H. E. Unalan, A. Kanwal. S. Miller, M. Chhowalla, *Appl. Phys. Lett.* **2005**, *87*, 203511; b) B. Pradhan, S. K. Batabyal, A. J. Pal, *Appl. Phys. Lett.* **2006**, *88*, 093106; c) S. Chaudhary, H. Lu, A. M. Muller, C. J. Bardeen, M. Ozkan, *Nano Lett.* **2007**, *7*, 1973.

[21] C. Li, Y. Chen, Y. Wang, Z. Iqbal, M. Chhowalla, S. Mitra, *J. Mater. Chem.* **2007**, *17*, 2406.

[22] a) W. Ma, C. Yang, X. Gong, K. Lee, A. J. Heeger, *Adv. Funct. Mater.* **2005**, *15*, 1617; b) G. Li, V. Shrotriya, J. Huang, Y. Yao, T. Moriarty, K. Emery, Y. Yang, *Nat. Mater.* **2005**, *4*, 864; c) Y. Kim, S. Cook, S. M. Tuladhar, S. A. Choulis, J. Nelson, J. R. Durrant, D. D. C. Bradley, M. Giles, I. Mcculloch, C.-S. Ha, M. Ree, *Nat. Mater.* **2006**, *5*, 197; d) H. Hoppe, N. S. Sariciftci, *J. Mater. Chem.* **2006**, *16*, 45.

[23] The clusterization of fullerene single components by lyophobic interaction has been reported. a) Y.-P. Sun, *Nature* **1993**, *365*, 398; b) Y. M. Wang, P. V. Kamat, L. K. Patterson, *J. Phys. Chem.* **1993**, *97*, 8793; c) Y.-P. Sun, B. Ma, C. E. Bunker, B. Liu, *J. Am. Chem. Soc.* **1995**, *117*, 12705; d) S. Nath, H. Pal, D. K. Palit, A. V. Sapre, J. P. Mittal, *J. Phys. Chem. B* **1998**, *102*, 10158; e) P. V. Kamat, S. Barazzouk, K. G. Thomas, S. Hotchandani, *J. Phys. Chem. B* **2000**, *104*, 4014; f) S. Barazzouk, S. Hotchandani, P. V. Kamat, *Adv. Mater.* **2001**, *13*, 1614; g) H. Hotta, S. Kang, T. Umeyama, Y. Matano, K. Yoshida, S. Isoda, H. Imahori, *J. Phys. Chem. B* **2005**, *109*, 5700; h) K. G. Thomas, M. V. George, P. V. Kamat, *Helv. Chim. Acta* **2005**, *88*, 1291.

[24] H. Imahori, *J. Mater. Chem.* **2007**, *17*, 31.

[25] a) H. Imahori, T. Hasobe, H. Yamada, P. V. Kamat, S. Barazzouk, M. Fujitsuka, O. Ito, S. Fukuzumi, *Chem. Lett.* **2001**, 784; b) T. Hasobe, Y. Kashiwagi, M. A. Absalom, J. Sly, K. Hosomizu, M. J. Crossley, H. Imahori, P. V. Kamat, S. Fukuzumi, *Adv. Mater.* **2004**, *16*, 975; c) T. Hasobe, P. V. Kamat, V. Troiani, N. Solladie, T. K. Ahn, S. K. Kim, D. Kim, A. Kongkanand, S. Kuwabata, S. Fukuzumi, *J. Phys. Chem. B* **2005**, *109*, 19; d) T. Hasobe, H. Imahori, P. V. Kamat, S. Fukuzumi, *J. Am. Chem. Soc.* **2003**, *125*, 14962; e) S. Kang, T. Umeyama, M. Ueda, Y. Matano, H. Hotta, K. Yoshida, S. Isoda, M. Shiro, H. Imahori, *Adv. Mater.* **2006**, *18*, 2549; f) H. Imahori, A. Fujimoto, S. Kang, H. Hotta, K. Yoshida, T. Umeyama, Y. Matano, S. Isoda, M. Isosomppi, N. V. Tkachenko, H. Lemmetyinen, *Chem. Eur. J.* **2005**, *11*, 7265; g) A. Kira, M. Tanaka, T. Umeyama, Y. Matano, G. Li, S. Ye, M. Isosomppi, N. V. Tkachenko, H. Lemmetyinen, H. Imahori, *J. Phys. Chem. C* **2007**, *111*, 13618; h) H. Imahori, M. Ueda, S. Kang, H. Hayashi, S. Hayashi, H. Kaji, S. Seki, A. Saeki, S. Tagawa, T. Umeyama, Y. Matano, K. Yoshida, S. Isoda, M. Shiro, N. V. Tkachenko, H. Lemmetyinen, *Chem. Eur. J.* **2007**, *13*, 10182.

[26] To avoid the precipitation of $(C_{60}+\text{f-SWNT})_m$, the absorption spectrum of the mixture of C_{60} and f-SWNT in the mixed solvent was measured using a 1 cm optical cuvette. The same volume of ODCB/acetonitrile (1:3, v/v) was further added to the solution before the measurement.

[27] Since we could obtain the only blurred FE-SEM images of the fibrils in Figure 4b,d, the average diameters of the fibrils may include an experimental error to some extent.

[28] The DLS measurement of $(C_{60}+\text{f-SWNT})_m$ in ODCB/acetonitrile showed the two particles with average diameters of 200 nm and 2000 nm. The small particle can be assigned to $(C_{60})_m$ (cluster **III**), whereas the large particle may originate from clusters **I** and **II**. The size and the distribution of large particle are not accurate because of the fibrous structure of cluster **I** and the network structure of cluster **II**.

[29] T. Hasobe, S. Fukuzumi, P. V. Kamat, *Angew. Chem.* **2006**, *118*, 769; *Angew. Chem. Int. Ed.* **2006**, *45*, 755.

[30] a) P. V. Kamat, K. G. Thomas, S. Barazzouk, G. Girishkumar, K. Vinodgopal, D. Meisel, *J. Am. Chem. Soc.* **2004**, *126*, 10757; b) S. Barazzouk, S. Hotchandani, K. Vinodgopal, P. V. Kamat, *J. Phys. Chem. B* **2004**, *108*, 17015; c) F. Itoh, I. Suzuki, K. Miyairi, *Jpn. J. Appl. Chem.* **2005**, *44*, 636.

[31] T. Umeyama, M. Fujita, N. Tezuka, N. Kadota, Y. Matano, K. Yoshida, S. Isoda, H. Imahori, *J. Phys. Chem. C* **2007**, *111*, 11484.

[32] H. Kataura, Y. Kumazawa, Y. Maniwa, I. Umezu, S. Suzuki, Y. Ohtsuka, Y. Achiba, *Synth. Met.* **1999**, *103*, 2555.

[33] A. M. Rao, P. C. Eklund, J.-L. Hodeau, L. Marques, M. Nunez-Regueiro, *Phys. Rev. B* **1997**, *55*, 4766.

[34] M. S. Dresselhaus, G. Dresselhaus, R. Saito, A. Jorio, *Phys. Rep.* **2005**, *409*, 47.

[35] The difference (10–20 nm) in the average diameters of the bundles of $(\text{f-SWNT})_m$ and cluster **I** in Figure 4b,d is slightly larger than that (6 nm) in Figure 6b and Figure 7a. This may result from the inaccuracy in the former case (ref. [27]) as well as the difference in the sample preparation.

[36] G. M. A. Rahaman, D. M. Guldi, R. Cagnoli, A. Mucci, L. Schenetti, L. Vaccari, M. Prato, *J. Am. Chem. Soc.* **2005**, *127*, 10551.

[37] a) F. Patolsky, Y. Weizmann, I. Willner, *Angew. Chem.* **2004**, *116*, 2165; *Angew. Chem. Int. Ed.* **2004**, *43*, 2113; b) L. Sheeney-Haj-Khia, B. Basnar, I. Willner, *Angew. Chem.* **2005**, *117*, 80; *Angew. Chem. Int. Ed.* **2005**, *44*, 78.

[38] a) K.-i. Okazaki, Y. Nakato, K. Murakoshi, *Phys. Rev. B* **2003**, *68*, 035434; b) A. Jorio, R. Saito, J. H. Hafner, C. M. Lieber, M. Hunter, T. McClure, G. Dresselhaus, M. S. Dresselhaus, *Phys. Rev. Lett.* **2001**, *86*, 1118; c) J. Zhao, J. Han, J. P. Lu, *Phys. Rev. B* **2002**, *65*, 193401.

[39] S. Demmig, H. Langhals, *Chem. Ber.* **1988**, *121*, 225.

Received: December 15, 2007
Published online: April 16, 2008

